Preparation and characterization of LaAlO$_3$

L. John Berchmans [a,*], S. Angappan [a], A. Visuvasam [a], K.B. Ranjith Kumar [b]

[a] Central Electrochemical Research Institute, Karaikudi 630006, Tamil Nadu, India
[b] Department of Physics, Thiagarajar College of Engineering, Madurai 625015, Tamil Nadu, India

Abstract

Lanthanum aluminate has been prepared by combustion synthesis process using nitrate salts of lanthanum and aluminium as cation precursors and urea as the fuel. The powder density and the compacted pellet density have been determined. Sintering process reduces the porosity of the pellets by the agglomeration process. The conductivity of LaAlO$_3$ increases with sintering temperature and the value is found to be 1.75 S cm^{-1} at 1000 °C. The dielectric constant and loss tangent values are found to decrease with the applied frequency. This may be due to the change in orientation and ionic effects resulted from the inertia of ions and molecular levels. The XRD studies reveal that the material is assigned to be a pseudocubic structure. The FTIR spectra show the higher frequency and lower frequency bands are assigned to AlO$_6$ octahedra in LaAlO$_3$. SEM micrographs divulge the presence of platelet aggregates into globular mass with larger surface area. The electrochemical polarization was performed for as synthesized and sintered LaAlO$_3$ materials in 0.5–2.0 M KOH. In general the corrosion kinetic parameters elucidate the fact that the green samples are found to be prone to corrosion than the sintered materials.
© 2007 Elsevier B.V. All rights reserved.

Keywords: Ceramics; Chemical synthesis; Powder diffraction; Electrochemical properties

1. Introduction

The development of advanced materials has found greater applications in traditional as well as sophisticated areas. Thus, the preparation of materials possessing desired properties, composition, structural and morphological features continues to be a challenge for materials scientists. Lanthanum aluminate is one of the important materials has potential applications in the areas of high frequency capacitors, magneto hydrodynamic generators, substrate for super conducting, ferro electric thin films and colossal magneto resistance [1–7]. The common method of preparation of LaAlO$_3$ is by solid state reaction method on mixing high purity aluminium oxide (Al$_2$O$_3$) and lanthanum oxide (La$_2$O$_3$) at high temperatures [8–10]. LaAlO$_3$ powder has also been synthesized by aqueous co-precipitation method [11,12] and aerosol furnace technique [13]. Several wet and soft chemical methods including polymerized complex method using citric acid and ethylene glycol route [14] have been tried. Poly Vinyl Alcohol (PVA) with metal nitrate synthesis [15], sol–gel

process [16–18], EDTA gel route [19,20], pyrolysis using triethanolamine [21] and combustion synthesis with urea as fuel [22,23] have also been reported.

From the literature, it can be seen that each method mentioned has certain merits and demerits on the synthesis process. The corrosion behavior of this material is one of the important properties in considering its application in the field of electrochemistry especially for electro catalysis, electrochemical energy systems and sensors. In view of the fact, an attempt has been made to synthesis LaAlO$_3$ by combustion synthesis and characterized for its physical and electrochemical properties in aqueous environments. This paper describes the results on the low temperature synthesis and the electrochemical characterization of the material in aqueous environments.

2. Experimental

Lanthanum aluminate was prepared by combustion synthesis using La(NO$_3$)$_3$·6H$_2$O and Al(NO$_3$)$_3$·9H$_2$O as cation precursors and CO(NH$_2$)$_2$ as the fuel. The combustion synthesis technique is based on the thermo chemical concepts used in propellant chemistry [15], in which different fuels such as tetra formyl triazine TFTA (C$_4$H$_{16}$N$_6$O$_2$), maleic hydrazide (C$_4$H$_4$N$_2$O$_2$), carbo hydrazide (CO(N$_2$H$_3$)$_2$) and glycine (NH$_2$CH$_2$COOH) have been used. All of these compounds contain nitrogen but differ in the reducing power and the amount of gases that generate, which obviously affects the characterization

* Corresponding author. Tel.: +91 4565 227550 59;
fax: +91 4565 227713/227779.
E-mail address: ljberchmans@yahoo.com (L. John Berchmans).

of the reaction product. The advantages of urea are that it has the lowest reducing power (total valencies +6), cheap, commercially available and produces the smallest volume of gases. The nitrate salts are favored as precursors because they serve as water-soluble at low temperature and nitrogen source for the synthesis. The reactants were dissolved in deionized water in a cylindrical quartz bowl. The bowl containing the solutions was placed on an open heater maintained at around 300 °C. Initially the solution boiled and dehydrated followed by decomposition, releasing copious amounts of heat and gases. The mixture slowly turned into a highly viscous gel. On further heating the gel swelled into a foam of fine flakes and got ignited with evolution of large quantity of gases yielding foamy powder of lanthanum aluminate (LA1). The foamy powders were then hand ground in an agate mortar and were calcined.

The finely ground lanthanum aluminate powders were screened by laser particle size analyzer (model MALVERN 3600 EC England). The transmitting source is He–Ne laser of 2 m in 362.8 nm wavelength. The complete range of particle size distribution measurement is 0.5–560 μm.

The powders were then pressed into pellets using a hydraulic press. These compacted pellets were sintered at high temperatures using an electrically heated furnace fitted with a digital temperature controller cum indicator and heated continuously up to 1000 °C holding at intermediate temperature of 700 °C for 8 h. The sintered samples were labeled as LA2 at 700 °C and LA3 at 1000 °C.

The powder density was determined using Archimedes principle with a pycnometer and xylene as a liquid medium. The following weights were taken and used in the density calculation:

Weight of the bottle = W_1 g: weight of the bottle + sample = W_2 g; weight of the bottle + sample + xylene = W_3 g; weight of the bottle + xylene = W_4 g; density of xylene = ρ_{sol}; density of sample = ρ

$$\rho = \frac{W_2 - W_1}{(W_4 - W_3) + (W_2 - W_1)} \times \rho_{sol}$$

A known amount of powder was filled in to a graduated cylinder of 10 ml capacity and the cylinder was tapped until the powder level remained unchanged. The volume occupied by the powder was noted. The ratio between the weight of the sample and the volume gave tap density.

The density of both green and sintered pellets has been calculated using weight and volume method.

The porosity of the pellet was calculated by liquid absorption method. In this method, a non-reactive liquid—glycerol (density = 1.261 gm cm^{-3}) is used to fill up the pores under vacuum. From the weight of the liquid entered into the pellet the volume can be calculated. Subsequently the porosity of the material can be computed from the measurable values of the size using the relationship

$$\text{Porosity} (\%) = \frac{\Delta W}{d} \times \frac{1}{\text{vol. of the sample}} \times 100$$

The frequency variations of AC conductivity of all samples were carried out at room temperatures from 100 Hz to 10 kHz with the help of a computerized LCRTZ test systems (VLCRTZ1P-model). For better ohmic contact, silver paste was applied to both the surfaces of pellet before being sand witched between the two electrodes of sample holder.

DC conductivity of the sintered specimens was measured as a function of temperature using four-probe method. Platinum wires were used as current collector and potential leads. The measurements were carried out from ambient temperature to 1000 °C for all the samples. The resistance was measured using a micro ohmmeter on heating and cooling cycles and the error was found to be less than 1%. The temperature was measured using a Cr–Al thermocouple and the rate of heating was controlled by a programmable temperature controller.

The X-ray powder diffraction patterns of green and sintered specimens were recorded using Cu Kα (α = 1.541 Å) radiation with 2θ values ranging from 20° to 70° in JEOL 8030 X-ray diffractometer. The lattice parameter 'a' is calculated directly using the equation,

$$a = d_{hkl}(h^2 + k^2 + l^2)^{1/2}$$

where 'hkl' is miller indices of the crystal structure.

The FT-IR spectra of the samples were recorded as KBr discs in the range 400–1000 cm^{-1} by using (FTIR—Perkin Elmer, UK Paragon-500) spectrometer.

A Scanning Electron Microscope (SEM) JEOL–JSM–3.5 CF-Japan make was employed for the morphological studies.

The potentiodynamic polarization studies were carried out with a three-electrode configuration, in 0.5–2.0 M KOH solution using a BAS 100 A (Bio Analytical Systems, U.S.A) electrochemical analyser. A platinum foil of large area (10 cm^2) was used as the counter electrode. A saturated calomel electrode (SCE) connected to the cell by a bridge with luggin capillary served as the reference electrode. The exposed surface area of the working electrode was 1 cm^2. Initially the working electrode was kept under open circuit potential (OCP) for 30 min to attain a stabilized (OCP) value. The polarization curves were recorded at ambient temperature (28 ± 2 °C) by fixing the potential of 300 mV on either direction of OCP, at the scan rate of 1 mV s^{-1}.

3. Results and discussion

3.1. Characterization

On examining the particle size of different powders, it is seen that the particle size is found to increase from 50 to 57 μm for LA1–LA3 samples, respectively.

Table 1 shows the values of tap density, pellet density and porosity for LA1–LA3. From the table, it is found that the density of the powder increased with increase in sintering temperature. Therefore, the sintering process plays a major role in the agglomeration process where the individual particles are made into dense by the expense of external energy. Since, the synthesized powders have high surface area with well-defined chemical composition with homogeneity they exhibit high sinterability. It is also noted that the porosity of the pellet is found to decrease with increase in sintering temperature. The decrease in porosity is mainly due to the agglomeration of the individual particles. The fine particles that are loosely placed form a bonding among them and grow into bigger size by the elimination of voids. The sinterability of oxide materials is occurred mainly through the liquid phase sintering process.

Fig. 1 represents the specific electrical conductivity vs. temperature for the samples LA2 and LA3. It can be seen from the figure, that the material LA3 possesses higher electrical conductivity than the LA2 sample. Below 600 °C, the materials show poor conductivity whereas at higher temperatures, a rapid increase in conductivity is noticed. These observations have been noticed from the values of conductivity 0.01 and 0.1 S cm^{-1} at 300 °C, and 0.5 and 1.75 S cm^{-1} at 1000 °C. It is ascertained that the sintering process is being responsible for the electrical conductivity of these compounds. It is attributed that during the process of sintering, the number of charge carriers as well as their mobility have been increased which are responsible for the conductivity of the compounds.

Fig. 2 depicts the Arrhenius plot of the samples LA2 and LA3. It is seen that, a rise in reciprocal of temperature, results in a linear increase in the specific resistivity of the material. The

Table 1
Physical properties of the sample

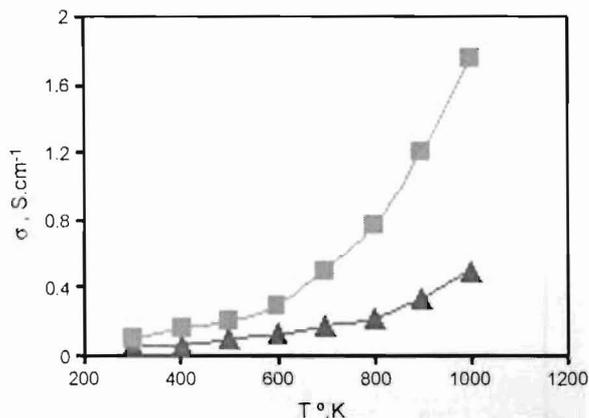| Sample	Tap density (g cm^{-3})	Pellet density (g cm^{-3})	Porosity (%)
LA1	1.067	2.762	26.8
LA2	1.629	3.184	23.0
LA3	2.160	4.025	17.7

Fig. 1. Plot of DC conductivity vs. temperature (▲) LA2 and (■) LA3.

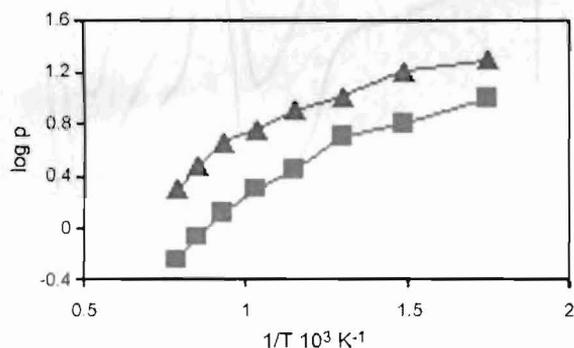Fig. 2. Plot of log ρ vs. $(1/T)10^3$ for (■) LA2 and (▲) LA3.

activation energy is calculated from the plot which is found to be 0.43 eV for LA2 and 0.28 eV for LA3. This observation clearly indicates the semiconducting nature of the materials.

It is reported that the conduction in perovskite compounds is mainly due to the number of charge carriers, mobility, phase transition, polaron hopping, redox species and decomposition reactions [24,25].

Fig. 3 shows the effect of applied frequency on the dielectric constant for the samples LA1, LA2 and LA3. It is seen that these materials initially exhibit a high value of dielectric constant, which further decreases with the applied frequency and reaches a minimum value. This observation is noticed in all the samples namely LA1, LA2 and LA3. The results in the decrease in dielectric constant with increase in frequency exhibits a constant
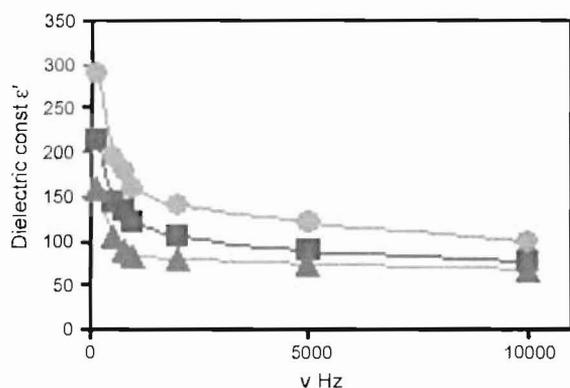

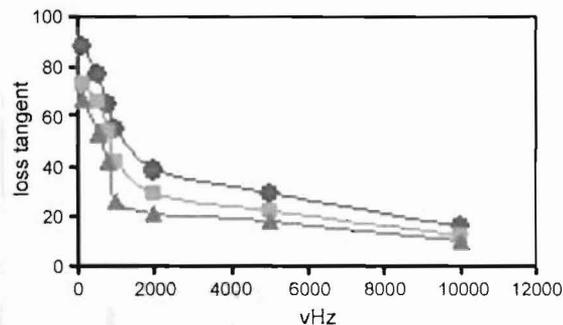Fig. 3. Plot of dielectric constant vs. frequency (●) LA1, (■) LA2 and (▲) LA3.

Fig. 4. Plot of loss tangent vs. frequency for (●) LA1, (■) LA2 and (▲) LA3.

value which may be due to the contribution of the ionic factor, which is a frequency-dependent phenomenon.

Fig. 4 shows the relationship between dielectric constant and the loss tangent of the samples. It is found that the loss tangent values are found to be high at lower frequency region and decline steeply on the increase in frequency. This may be mainly due to the loss of both ionic and electronic polarizations at lower frequency regions, whereas at the higher frequency regions the loss tangent is mainly due to the ionic vibrations. This behavior may due to the change in orientation and ionic effects resulted from the inertia of the ions and molecular levels.

Fig. 5(a–c) shows the X-ray diffraction patterns of LA1, LA2 and LA3, respectively. The XRD pattern of LA1 sample has shown amorphous peaks which indicate the incomplete phase formation of lanthanum aluminate. Sample LA3 exhibits the well-defined sharp peaks indicating the phase formation of $LaAlO_3$ which is confirmed from the JCPDS Card No. 31-0022 [26]. The 'd' spacing for the recorded peaks are calculated according to Bragg's law. These values are well agreement with the calculated and observed 'd' values. The pattern is matched with the characteristic reflection of lanthanum aluminate. The crystal structure of the sample whose lattice constant $a = 3.77$ Å is well agreeing with the reported data ($a = 3.79$ Å) [27]. From the data, it can be concluded that the structure may be of pseudocubic in nature.

The FTIR spectra for LA1, LA2 and LA3 which are recorded in the range 400–1000 cm^{-1} are shown in Fig. 6(a–c). From the spectra, it is noticed that the higher frequency band γ_1 has a values of 668.04, 662.39 and 663.72 cm^{-1} for LA1, LA2 and LA3 samples, respectively. The lower frequency range the band γ_2 appeared at 447.38, 448.1 and 450.68 cm^{-1} for LA1, LA2 and LA3 samples, respectively. These bands are assigned to AlO_6 octahedra in $LaAlO_3$ [28].

The scanning electron micrographs of the samples are shown in Fig. 7(a–c). Fig. 7(a), for LA1 shows irregular aggregates of crystallites spread over the entire area. Fig. 7(b and c) for LA2 and LA3 samples depicts the transformation of the crystallites into a dense mass with a reduction in porosity on sintering process.

3.2. Corrosion kinetic parameters

The electrochemical polarization curves for the as synthesized and sintered $LaAlO_3$ materials in 0.5–2.0 M KOH solutions

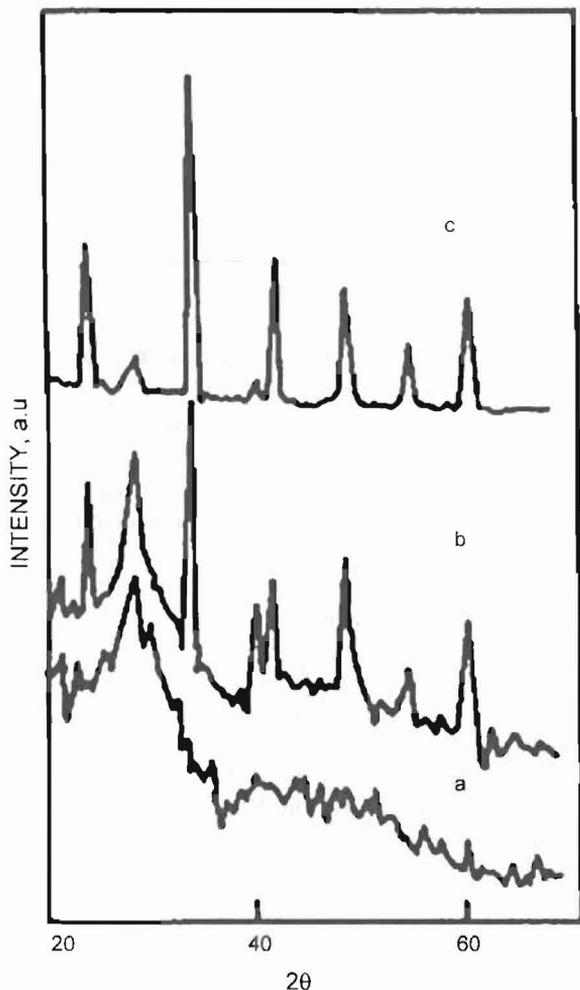Fig. 5. XRD pattern of (a) LA1, (b) LA2 and (c) LA3 samples.

Fig. 6. FTIR spectra of (a) LA1, (b) LA2 and (c) LA3 samples.

are presented in Figs. 8–10. The corrosion kinetic parameters such as corrosion current (I_{corr}), corrosion potential (E_{corr}), Tafel slopes (b_a and b_c) for the green and sintered $LaAlO_3$ samples are presented in Table 2. For the green sample, it is found that the E_{corr} values are shifted from lower value (125.2 mV) to higher value on increase in concentration of KOH solution. On increase in concentration of the electrolytic the E_{corr} values are found to
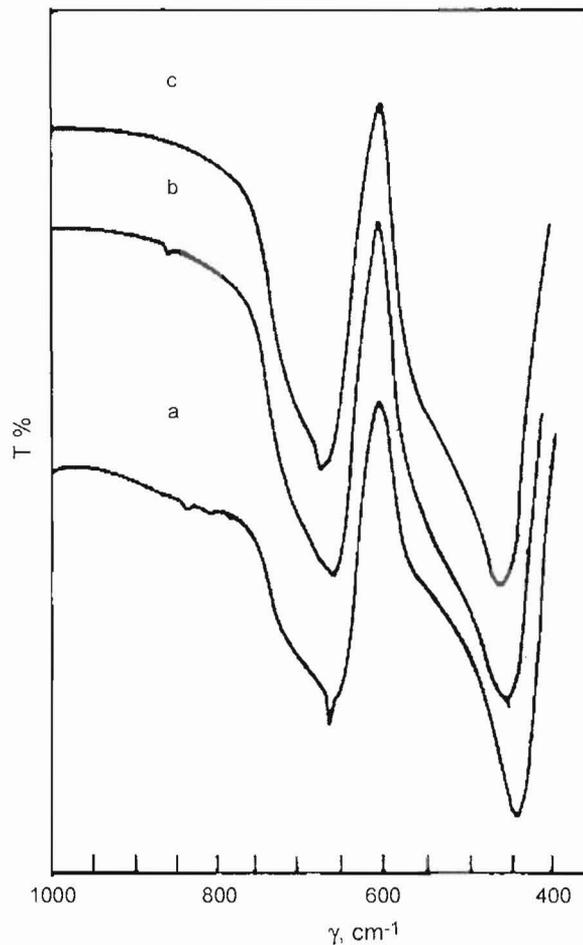
be more for green samples than the sintered materials. On comparing the values of E_{corr}, it is found that the values are less positive for the materials sintered at 700 °C than at 1000 °C. From the observations, it could be seen that the materials sintered at higher temperatures exhibit more resistance to corrosion in alkali solutions. This behavior is mainly due to the formation of a passive film on the surface of the material. Similar behavior has also been noticed on seeing the values of I_{corr} which are found to decrease for the sintered materials. On examining the

Table 2
Corrosion kinetic parameters of $LaAlO_3$

Sample	Concentration of KOH (M)	E_{corr} (mV)	I_{corr} ($\mu A\,cm^{-2}$)	b_a (mV)	b_c (mV)
LA1	0.5	125.2	1.2606	171.3	−119.9
	1.0	145.2	1.9408	132.0	−105.8
	1.5	141.4	1.6717	140.1	−128.2
	2.0	148.0	1.7434	126.6	−111.5
LA2	0.5	107.2	0.0550	205.9	−180.0
	1.0	118.0	0.0801	199.2	−199.3
	1.5	123.3	0.1137	215.8	−183.6
	2.0	123.9	0.1886	276.6	−137.0
LA3	0.5	100.5	0.0373	263.4	−143.1
	1.0	86.9	0.0362	164.2	−185.5
	1.5	109.8	0.0926	179.0	−176.0
	2.0	111.9	0.1170	136.9	−139.1

Fig. 7. SEM micrographs of (a) LA1, (b) LA2 and (c) LA3 samples.

Fig. 8. Polarization curve of LaAlO₃ green sample in (1) 0.5, (2) 1.0, (3) 1.5 and (4) 2.0 M KOH.

Fig. 9. Polarization curve of LaAlO₃ sintered at 700 °C in (1) 0.5, (2) 1.0, (3) 1.5 and (4) 2.0 M KOH.

Fig. 10. Polarization curve of LaAlO₃ sintered at 1000 °C in (1) 0.5, (2) 1.0, (3) 1.5 and (4) 2.0 M KOH.

Tafel slopes, it could be seen that the anodic Tafel slope is always found to be more positive than the cathodic Tafel slope irrespective of sintering temperature. On considering the b_c value for the sintered materials they are found to be less negative than the green samples. This observation infers that the hydrogen evolution reaction is being retarded by the formation of a protective passive film on the surface of the materials.

In general the corrosion kinetic parameters elucidate the fact that the green samples are more prone to corrosion than the sintered LaAlO₃ materials. It is emphasized that materials with high corrosion resistance is well suited when they are indented for electrochemical applications.
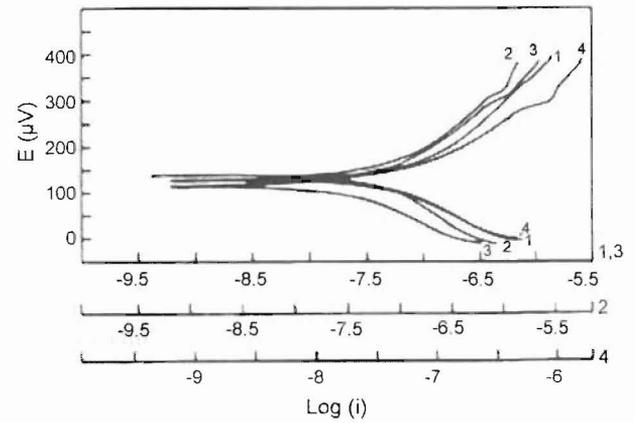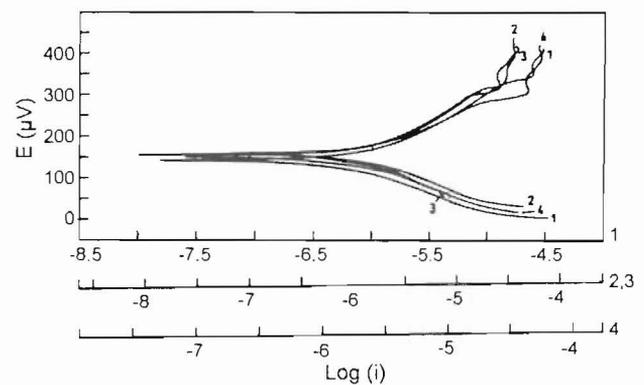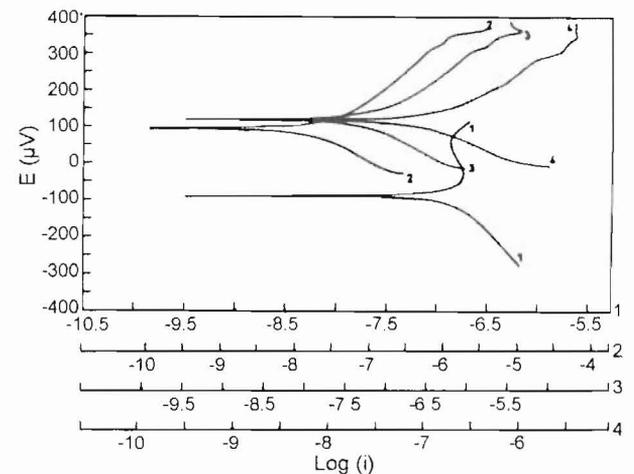
4. Conclusion

Combustion synthesis is found to be a convenient method for the preparation of pure LaAlO₃ powders at lower temperatures. On sintering process, the density of the pellets shows an increase in density with lesser porosity. The specific conductivity of the materials has a direct relationship with sintering temperature as

well as with measuring temperature. From the calculated lattice constant value of 3.77 Å the material exhibits a pseudocubic structure. From the AC electrical conductivity studies, it is seen that the synthesized $LaAlO_3$ is identified as a semiconductor material. The prepared $LaAlO_3$ compound has possessed good physical and electrochemical properties which can be utilized as electrode materials in aggressive environments.

Acknowledgements

References

[1] G.W. Berkstresser, A.J. Valentino, C.D. Brandle, J. Cryst. Growth 128 (1993) 684.
[2] G.Y. Sung, K.Y. Kang, S.C. Park, J. Am. Ceram. Soc. 74 (1991) 437.
[3] T.Y. Chen, K.Z. Fung, J. Alloys Compd. 368 (2004) 106.
[4] M. Nieminen, T. Sajavaara, E. Rauhala, M. Putkonen, L. Niisisto, J. Mater. Chem. 11 (2001) 2340.
[5] T.L. Nguyen, M. Donkiya, S. Wang, H. Togawa, T. Hashimoto, Solid State Ionics 130 (2000) 229.
[6] B.J. Kennedy, C.J. Howard, A.K. Prodlosantoso, B.C. Chakoumakos, Mater. Sci. Process. 74 (2002) 1660.
[7] R. Guo, D. Guo, Y. Chen, Z. Yang, Q. Yuan, Ceram. Int. 28 (7) (2002).
[8] C.S. Hsu, C.L. Huang, Mater. Res. Bull. 36 (2001) 1939.
[9] M.L. Keith, R. Roy, Am. Miner. 39 (1954) 1.
[10] S.J. Schneider, R.S. Rolk, J.L. Waring, J. Res. Mater. Bur. Stand. 65A (1961) 345.
[11] M.A.C.G. Van De Graaf, J.H.H. Ter matt, A.J. Burggraaj, J. Mater. Sci. 20 (1985) 1407.
[12] W. Li, M.W. Shi, J.L. Zhou, Mater. Lett. 58 (2004) 365.
[13] B.C. Lux, R.D. Clark, A. Salazar, L.K. Sveum, M.A. Krebs, J. Am. Ceram. Soc. 76 (1993) 2669.
[14] M. Kakihan, T. Okubo, J. Alloys Compd. 266 (1998) 129.
[15] A.K. Adak, P. Pramanik, Mater. Lett. 30 (1997) 269.
[16] M. Chronia, J. Pinkas, I. Pakutinskiene, A. Begankiene, A. Kareiva, Ceram. Int. 31 (2005) 1123.
[17] S.N. Koc, F. Oksuzomer, E. Yasav, S. Akturk, M.A. Gurkaynak, Mater. Res. Bull. 41 (2006) 2291.
[18] A. Barrera, S. Fuentes, M. Viniegra, M. Avalos-Borja, N. Bogdan Chikova, J.C. Molina, Mater. Res. Bull. 42 (2007) 640.
[19] Y. Xu, G. Huang, H. Long, Ceram. Int. 29 (2003) 837.
[20] D. Zhou, G. Huang, X. Chen, J. Xu, S. Gong, Mater. Chem. Phys. 84 (2004) 33.
[21] S. Ran, L. Gao, Ceram. Int., in press.
[22] J.J. Kingsley, K.C. Patil, Mater. Lett. 6 (1988) 427.
[23] M.D. Shaji Kumar, T.M. Srinivasan, P. Ramasamy, C. Subramanian, Mater. Lett. 25 (1995) 171.
[24] G. Raj Mohan, R. Kalai Selvan, R. Saraswathi, L. John Berchmans, C.O. Augustin, J. Mater. Sci. Technol. 11 (3) (2003) 22.
[25] D. Lybye, F.W. Poulsen, M. Mogensen, Solid State Ionics 128 (2000) 91.
[26] Powder diffraction file, Card no 31-22 Joint Committee on Powder Diffraction Standards (JCPDS), Pennsylvania (1988).
[27] J.Y. Park, G.M. Choi, Solid State Ionics 154/155 (2002) 535.
[28] M. Couzi, P.V. Huong, J. Chim. Phys. Physico-Chim. Biol. 69 (1972) 1339.